Highly Efficient Organic Solar Cells with Improved Stability Enabled by Ternary Copolymers with Antioxidant Side Chains

Ao Song[1,‡], Qiri Huang[1,‡], Chunyang Zhang[1], Haoran Tang[1], Kai Zhang[1], Chunchen Liu[1,†] Fei Huang[1,†] and Yong Cao[1]

[1]Institute of Polymer Optoelectronic Materials and Devices, State Key Laboratory of Luminescent Materials and Devices, South China University of Technology (SCUT), Guangzhou, 510640.

E-mail: mscliu@scut.edu,cn, msfhuang@scut.edu.cn

Methods

Materials. Acceptor Y6 was purchased from VOLT-AMP OPTOELECTRONICS TECH. CO., LTD. and was used directly. The reagents and solvents used in the experiments were purchased from commercial sources such as Sigma Aldrich, Energy Chemistry, and *J&K* chemical, and were used directly unless otherwise noted.

Synthetic Procedures of Intermediates and Polymers

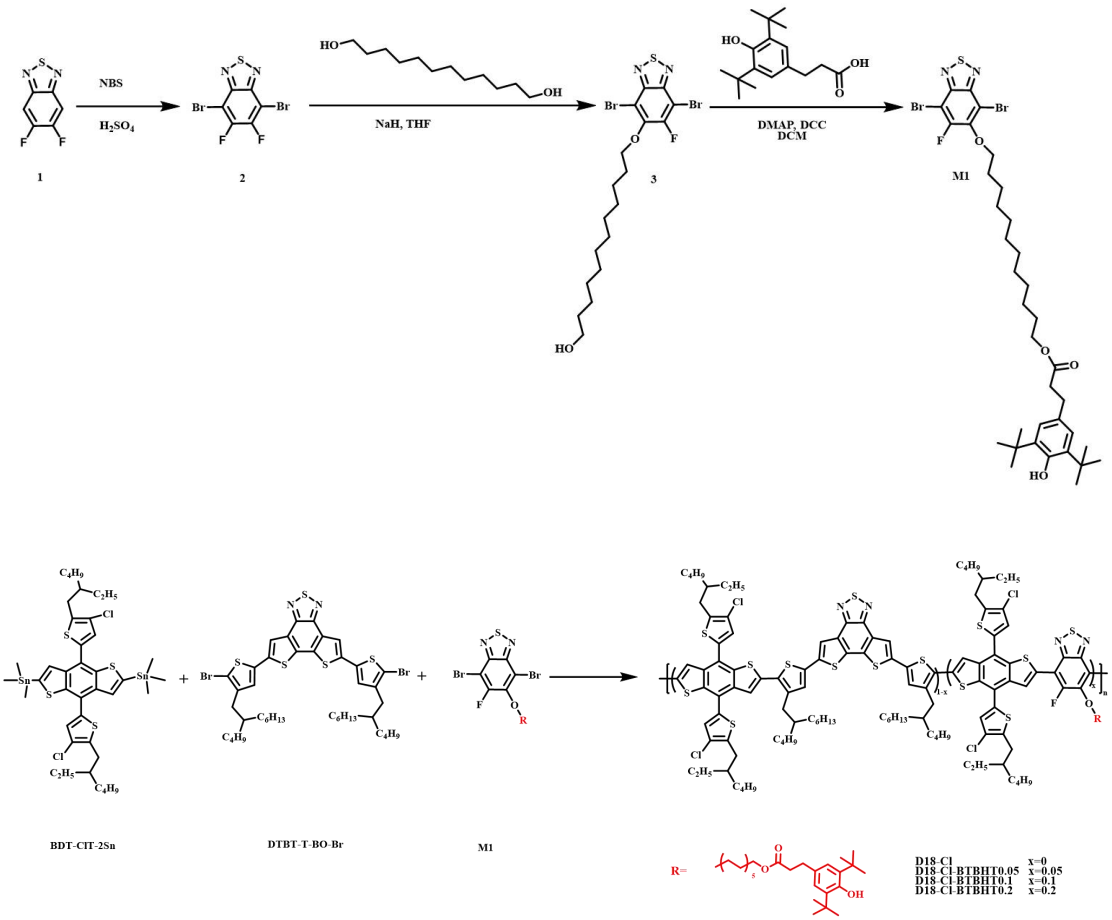

Scheme S1. Synthetic routes of M1 and D18-Cl-BTBHTx.

4,7-Dibromo-5,6-difluorobenzo[c][1,2,5]thiadiazole (2):

Under an argon atmosphere, compound 1 (1g, 5.8 mmol) was dissolved in 50 mL of concentrated sulfuric acid. Then 4.57 g (25.5 mmol) of N-bromosuccinimide (NBS) was added and the reaction mixture was slowly heated to 50 °C for 4 h. The reaction procedure was monitored by thin film chromatography (TLC) in real time. After the

complete consumption of compound 1, the mixture was cooled to room temperature and then poured into the ice water. The precipitate was collected by filtration and washed with deionized water. Subsequently, the resulting white solid was dissolved in dichloromethane and washed with saturated brine for 3 times. The organic phase was dried with anhydrous magnesium sulfate, and then concentrated. The product 2 was purified by silica gel column chromatography with a yield of 57%.

^{1}H NMR (400 MHz, Chloroform-d) δ 7.26 (s, 1H).

^{13}C NMR (126 MHz, Chloroform-d) δ 152.94, 152.78, 150.86, 150.69, 148.88, 148.86, 148.84, 99.57, 99.47, 99.40, 99.34, 99.28.

12-((4,7-dibromo-6-fluorobenzo[c][1,2,5]thiadiazol-5-yl)oxy)dodecan-1-ol (3)：

Under an argon atmosphere, 1,12-dodecanediol (0.92 g, 4.5 mmol) was dissolved in 60 mL of tetrahydrofuran solution, and then 60% sodium hydride (0.14 g, 3.6 mmol) was added. The reaction mixture was stirred at 50 °C for 3 h, followed by which compound 2 (1.0 g, 3.0mmol) was added. The mixture was stirred at 50 °C overnight. The reaction mixture was poured into deionized water, and extracted with dichloromethane. The organic phase was collected, dried with anhydrous magnesium sulfate, and concentrated. The mixture was further purified by column chromatography with petroleum ether and methylene chloride (1:3 vol%) as eluent. The product was obtained with a yield of 58%.

^{1}H NMR (400 MHz, Chloroform-d) δ 4.24 (t, J = 6.4 Hz, 2H), 3.65 (t, J = 6.7 Hz, 2H), 1.89 (t, J = 7.4 Hz, 2H), 1.42 – 1.23 (m, 19H).

^{13}C NMR (126 MHz, Chloroform-d) δ 157.70, 155.64, 149.98, 149.45, 149.29, 149.14, 149.10, 106.21, 98.66, 98.47, 75.82, 75.78, 75.15, 63.11, 32.81, 30.27, 30.12, 29.59, 29.55, 29.52, 29.43, 29.28, 25.76, 25.75.

12-((4,7-dibromo-6-fluorobenzo[c][1,2,5]thiadiazol-5-yl)oxy)dodecyl3-(3,5-di-tert-butyl-4-hydroxyphenyl)propanoate (M1):

Under an argon atmosphere, compound 2 (0.9 g, 1.76 mmol) was dissolved in 60 mL

of dichloromethane solution. 3-(3,5-di-tert-butyl-4-hydroxyphenyl) propionic acid (0.54 g, 1.93 mmol) and 4-dimethylaminopyridine (0.023 g, 0.193 mmol) were added sequentially. The color of the resulting solution gradually became pale yellow. Then the solution temperature was cooled to 0 °C and *N*, *N*'-dicyclohexyl carbon diimide (0.4 g, 1.93 mmol) was added. The color changed from light yellow to milky white, and the solution was restored to room temperature and stirred overnight. The reaction solution was filtered and the filtrate is collected. The mixture was further purified by column chromatography with petroleum ether and methylene chloride (2:1 vol%) as the eluent. The product M1 was obtained as the pale yellow liquid product with a yield of 82%.

^{1}H NMR (400 MHz, Chloroform-d) δ 6.99 (s, 2H), 5.07 (s, 1H), 4.23 (t, *J* = 6.5 Hz, 2H), 4.07 (t, *J* = 6.8 Hz, 2H), 2.87 (t, *J* = 8.0 Hz, 2H), 2.59 (dd, *J* = 9.1, 7.0 Hz, 2H), 1.89 (t, *J* = 7.5 Hz, 2H), 1.62 (t, *J* = 6.7 Hz, 2H).

^{13}C NMR (126 MHz, Chloroform-d) δ 173.37, 152.13, 149.98, 135.87, 131.16, 124.77, 75.81, 75.77, 64.62, 36.52, 34.30, 31.03, 30.31, 30.12, 29.55, 29.53, 29.51, 29.29, 29.27, 28.65, 25.92, 25.76.

Synthesis of the polymers (D18-Cl-BTBHT*x*):

DTBT-T-BO-Br (0.1–0.1*x* mmol), M1 (0.1*x* mmol), and BDT-ClT-2Sn (0.1 mmol) (*x* = 0 for D18-Cl; *x* = 0.05 for D18-Cl-BTBHT0.05; *x* = 0.1 for D18-Cl-BTBHT0.1; *x* = 0.2 for D18-Cl-BTBHT0.2) were dissolved in chlorobenzene (2.5 mL) under argon protection. $Pd_2(dba)_3$ (3.0 mg) and tri(o-tolyl)phosphine (8.0 mg) were added. The mixtures were stirred at 110 °C for 48 hours, after which 2-(tributylstannyl)thiophene and 2-bromothiophene were sequentially added with 2 hours interval as end-capping agents. After the mixture was cooled to room temperature, the product was precipitated in methanol and filtered. Then the precipitate was purified by Soxhlet extraction with acetone, hexane, dichloromethane and chloroform in sequence. The chloroform fraction was collected and concentrated, which was then precipitated into methanol and filtered. The collected precipitate was dried under vacuum for 48 h to obtain a black-red fiber-like product.

High-temperature Gel Permeation Chromatography (GPC). Molecular weights of the polymers were measured on an Agilent Technologies PL-GPC 220 in 1,2,4-trichlorobenzene at 150 °C using a calibration curve of polystyrene standards.

NMR. ^{1}H NMR test of 2, 3 and M1 were conducted on a Bruker AV-400 MHz spectrometer in $CDCl_3$ at 25 °C. ^{13}C NMR test of 2, 3 and M1 were conducted on a Bruker AV-500 MHz spectrometer in $CDCl_3$ at 25 °C. ^{1}H NMR test of D18-Cl-BTBHT*x* were conducted on a Bruker AV-400 MHz spectrometer in 1,1,2,2-$C_2D_2Cl_4$ at 80 °C.

Differential Scanning Calorimetry (DSC). DSC curves were acquired from DSC 2500 with samples of 2-3 mg under nitrogen flow at heating and cooling rates of 10 °C min^{-1}.

Thermal Gravimetric Analyzer (TGA). TGA measurements were measured on TGA5500 with samples of 5-6 mg under nitrogen flow at heating and cooling rates of 10 °C min^{-1}.

UV-vis absorption spectra. UV-vis spectra were recorded on a SHIMADZU UV-3600 spectrophotometer from 300 to 1000 nm.

Cyclic Voltammetry (CV). CV measurement was conducted on a CHI660A Electrochemical Workstation, with ferrocene/ferrocenium (Fc/Fc^+) as the calibration standard. A 0.1 M acetonitrile solution of tetrabutylammonium hexafluorophosphate (TBAPF6) was used as electrolyte, in which a saturated calomel electrode, a platinum wire and a glass carbon worked as reference electrode, counter electrode and working electrode, respectively. The energy levels were calculated according to the following equations: $E_{HOMO} = -(E_{OX} + 4.41)$ eV and $E_{LUMO} = -(E_{RE} + 4.41)$ eV, where E_{OX} and E_{RE} are the onset oxidation potential and onset reduction potential of measured

samples, respectively.

Device fabrication and characterization. The devices were fabricated based on the structure of ITO/PEDOT:PSS/Active layer/PNDIT-F3N/Ag. The patterned indium tin oxide (ITO) glass substrates were cleaned by detergent, deionized water, and isopropanol sequentially, and then dried at 65℃ in a baking oven overnight. After UV-ozone treatment for 4 min, the ITO substrates were coated with 40 nm thick PEDOT:PSS, and then annealed in air at 150°C on a hot plate for 15 min. Next, the substrates were transferred into a nitrogen-filled protected glove box, and the solution of polymer donors: Y6 (1:1.4, w/w, dissolved by chloroform, with a total concentration of 8.4 mg mL^{-1}) were spin-coated at 3000 rpm to produce 110 nm active layer. Here, polymer donors were D18-Cl, D18-Cl-BTBHT0.05, D18-Cl-BTBHT0.1, and D18-Cl-BTBHT0.2. Then, a thin layer of PNDIT-F3N was coated from its methanol solution (2%-5% (v/v) acetic acid) (1 mg mL^{-1}) onto the active layer to form an electron transport layer. Finally, 100 nm Ag was thermally deposited on top of all devices through a mask under a vacuum of ~1×10^{-7} mbar. The effective area of the devices was 0.04 cm^2.

***J-V* and EQE.** The current density-voltage (*J-V*) characteristics of the devices were measured under 1 sun, AM 1.5 G solar simulator (Taiwan, Enlitech SS-F5) by using a computer-controlled Keithley 2400 Source Meter. The light intensity was calibrated by a China General Certification Center certified reference silicon solar cell (Enlitech) before test, giving a 100 mW cm^{-2} light intensity during test. The external quantum efficiency (EQE) data were recorded with a QE-R test system (Enlitech).

Light operational stability measurements. Test under encapsulation: The devices were encapsulated with epoxy glue and glass in N_2 protected box. Then the devices were transferred into atmosphere, where the temperature was around 25 ℃ and humidity between 30-40%, for the stability test. Light exposure was performed using a LED source with light intensity calibrated to achieve the same device performance

measured by the standard AM 1.5 G solar simulator. Test without encapsulation: Devices without encapsulation was measured under the ambient atmosphere with the temperature of 25 ℃ and the humidity of 30-40%. Light exposure was performed using an LED light source and the light intensity was calibrated as described above.

Space-charge-limited current measurement. The charge transport properties of blend films were investigated by a space-charge-limited current method. The hole-only devices were fabricated with a configuration of ITO/PEDOT:PSS/BHJ/MoO_3/Ag, while the electron-only devices were fabricated with a structure of ITO/ZnO/BHJ/PNDIT-F3N/Ag. The mobility was determined by fitting the dark current with the Mott-Gurney law described as: $J = (9/8)\varepsilon_0\varepsilon_r\mu((V^2)/(d^3))$, where J is the current density, μ is the zero-field mobility, ε_0 is the permittivity of free space, ε_r is the relative permittivity of the material, d is the thickness of the active layers, and V is the effective voltage. The effective voltage was obtained by subtracting the built-in voltage (V_{bi}) and the voltage drop (V_s) from the series resistance of the whole device except for the active layers from the applied voltage (V_{appl}), $V = V_{appl} - V_{bi} - V_s$. ($V_{bi}$ = 0 and $V_s = 10 \times I$, where the value 10 is the resistance of MoO_3 and I is the current of the devices in this work). The hole and electron mobilities can be calculated from the slope of the $J^{1/2}$-V curves.

GIWAXS. GIWAXS was measured using HomeLab, A Japanese Rigaku brand, with an operating wavelength of 1.5405 Å. The Hypix-6000 photon direct reading detector is adopted with the pixel size of 0.1mm × 0.1mm. The distance of sample to detector was 64.2525 mm. The wavelength of X-ray is 1.5405 Å, corresponding to a beam energy of 8.04831 keV. The data were processed and analyzed by Nika software package. Gaussian peak fitting was used to obtain peak position and full width at half maximum (FWHM) of the scattering peak. Packing distance d can be calculated using $d = 2\pi/q$, where q is the corresponding peak position. Crystal coherence length (CCL) was calculated from GIWAXS line-cut by the Scherrer equation: $CCL = 2\pi K / \Delta q$;

where Δq is FWHM of the scattering peak and Scherrer constant K is often reported to be ~0.9[1].

Morphology characterizations: AFM images were tested by a Digital Instrumental DI Multimode Nanoscope III in a taping mode. TEM imagines were tested by a JEM-2100F instrument.

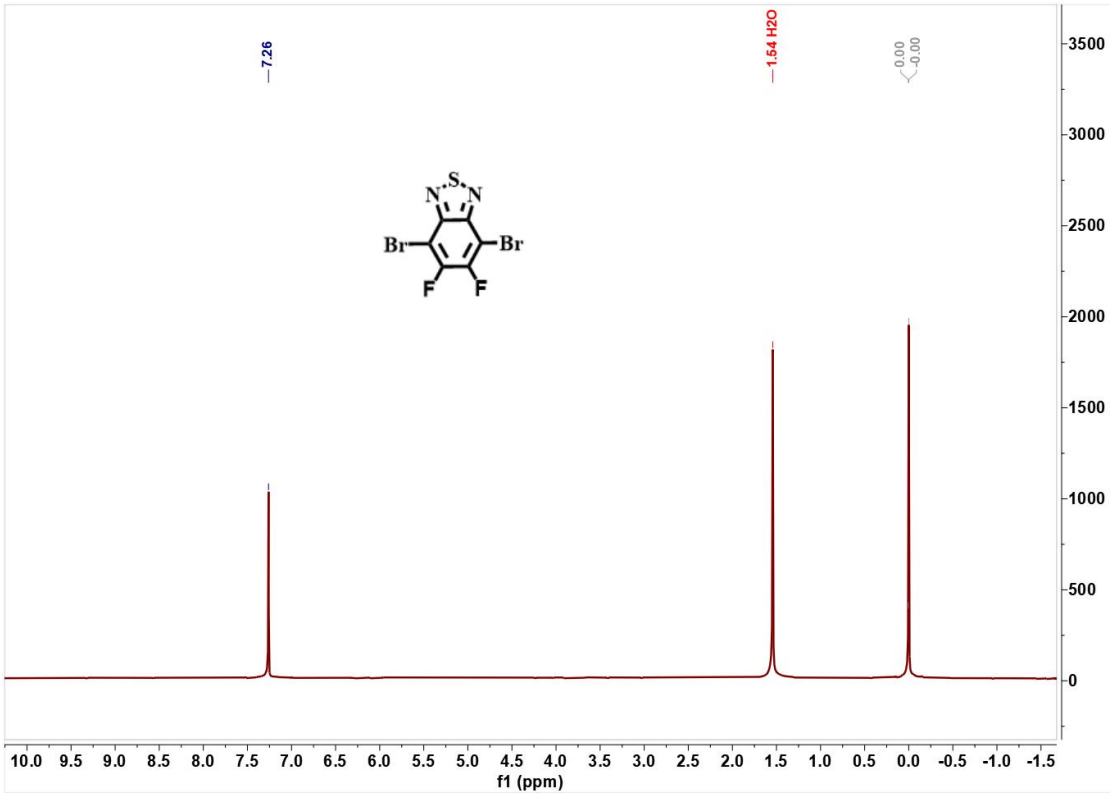

Fig. S1. ^{1}H NMR spectra of compound 2 ($CDCl_3$).

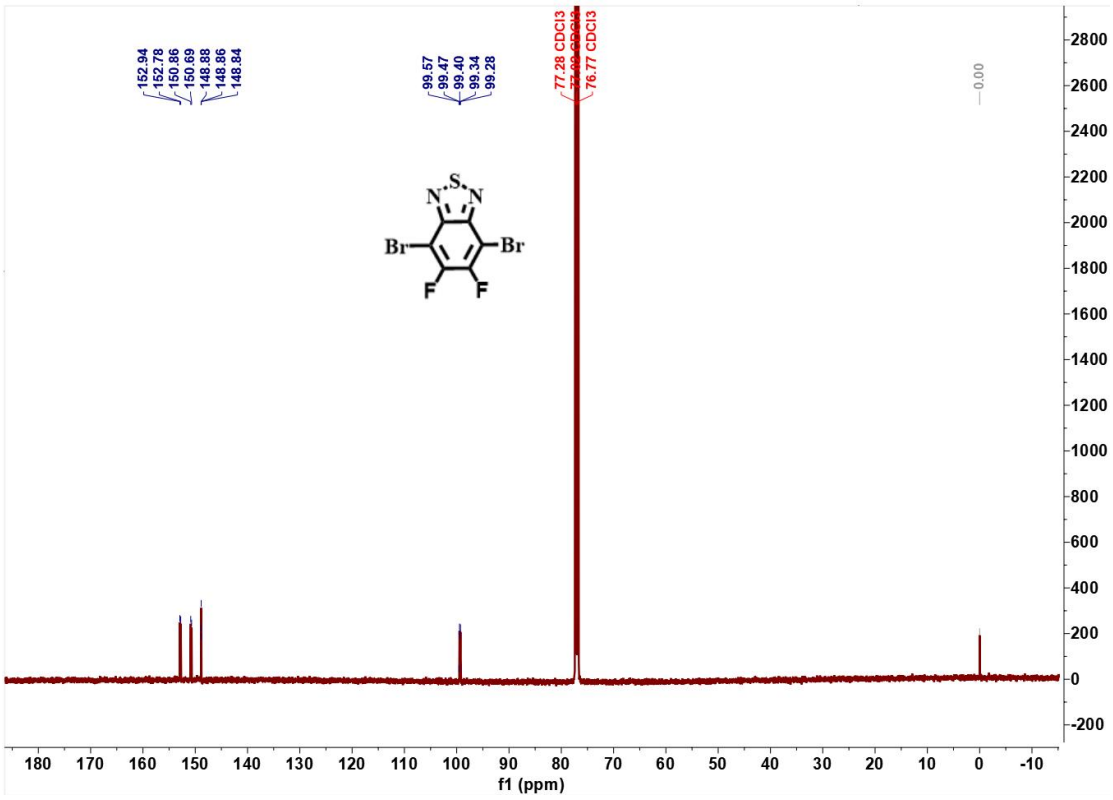

Fig. S2. ^{13}C NMR spectra of compound 2 ($CDCl_3$).

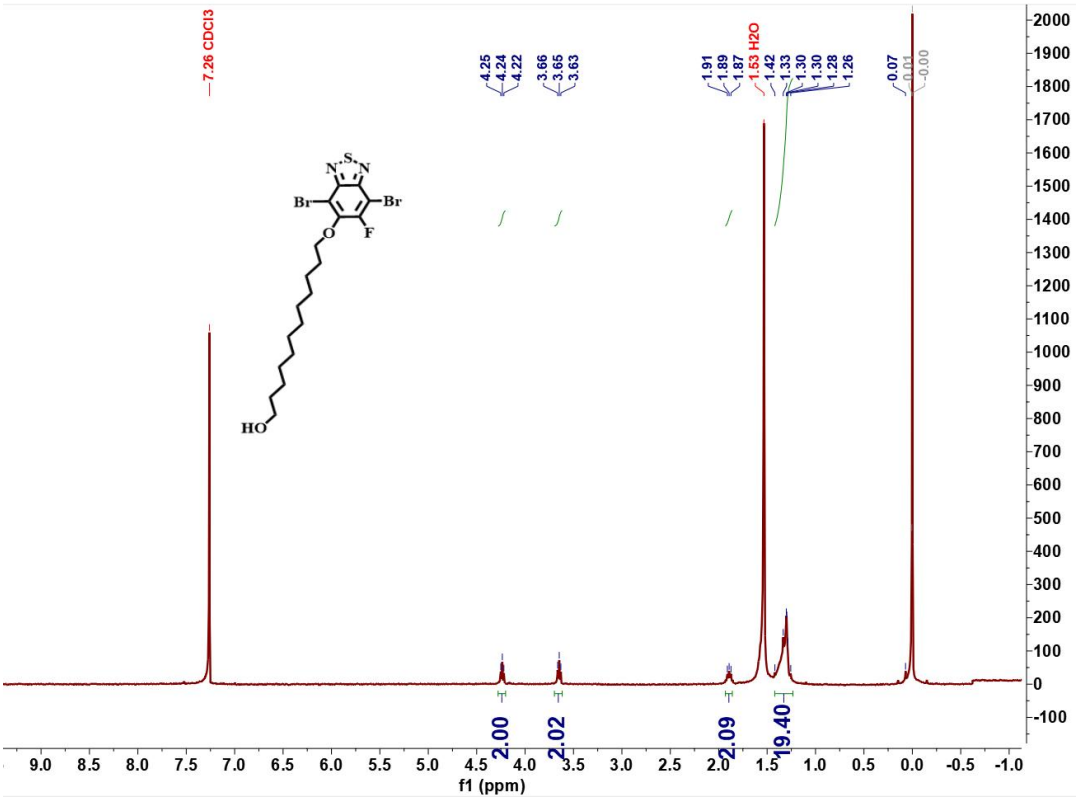

Fig. S3. ^{1}H NMR spectra of compound 3 ($CDCl_3$).

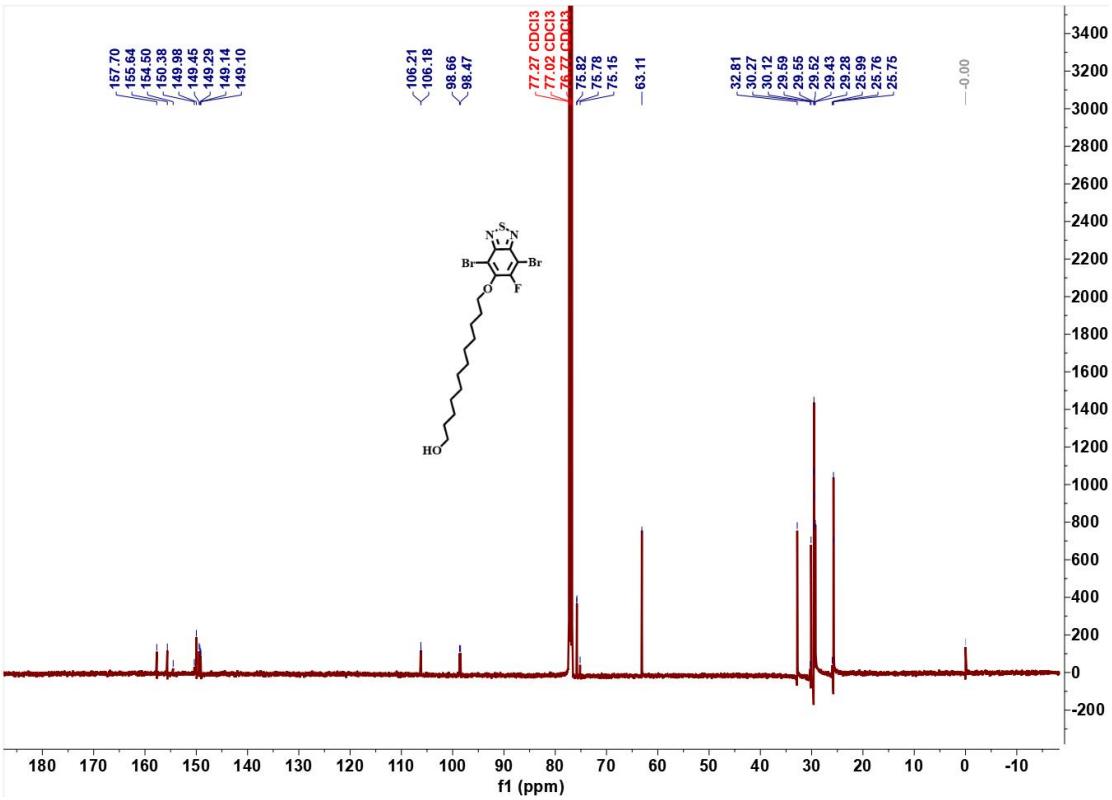

Fig. S4. ^{13}C NMR spectra of compound 3 ($CDCl_3$).

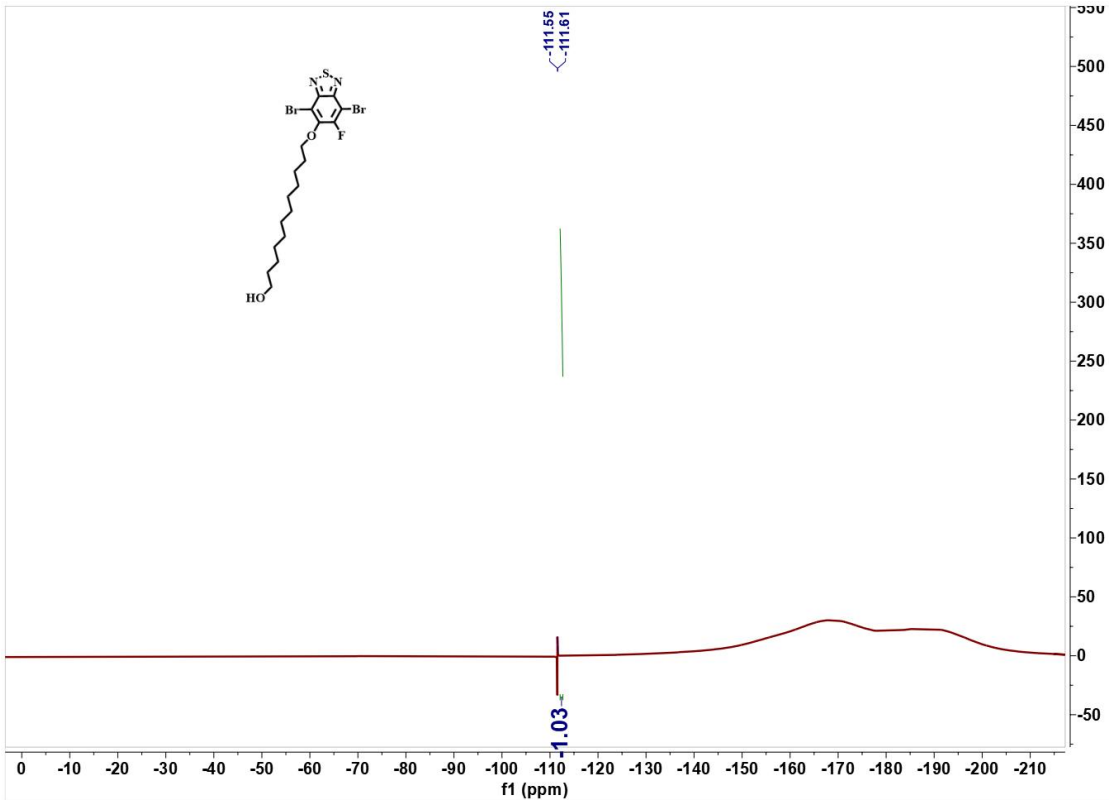

Fig. S5. ^{19}F NMR spectra of compound 3 ($CDCl_3$).

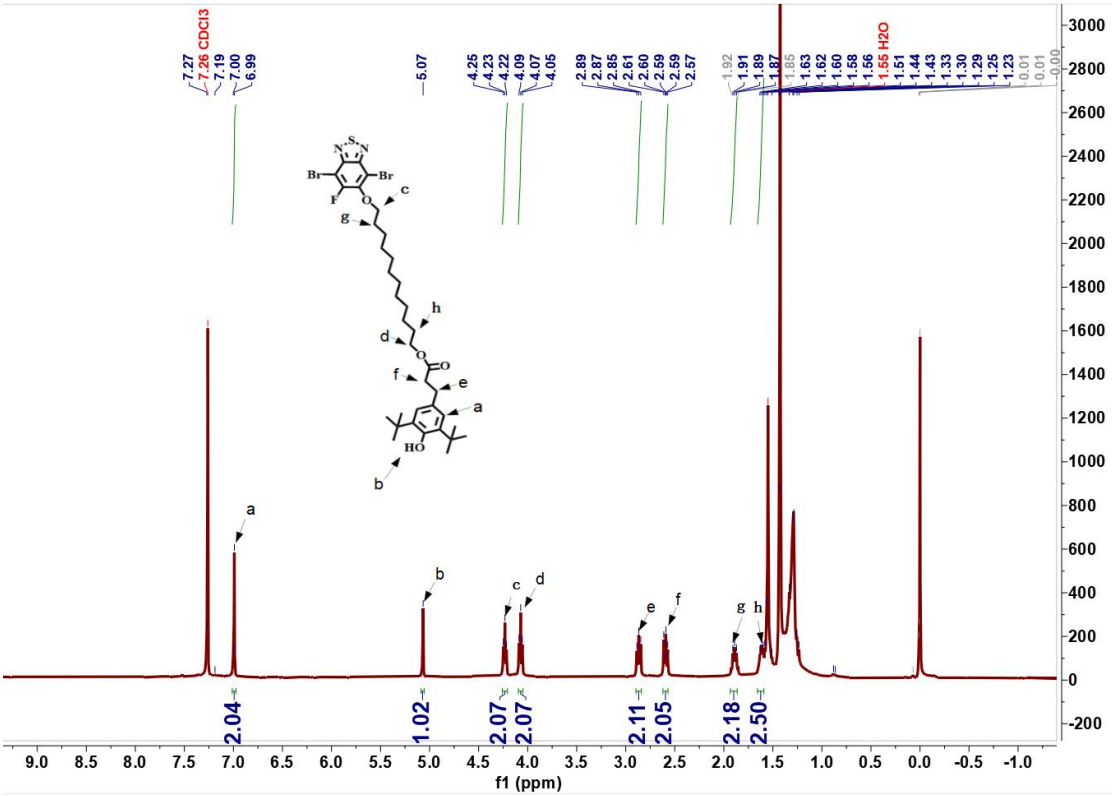

Fig. S6. ^{1}H NMR spectra of compound M1 ($CDCl_3$).

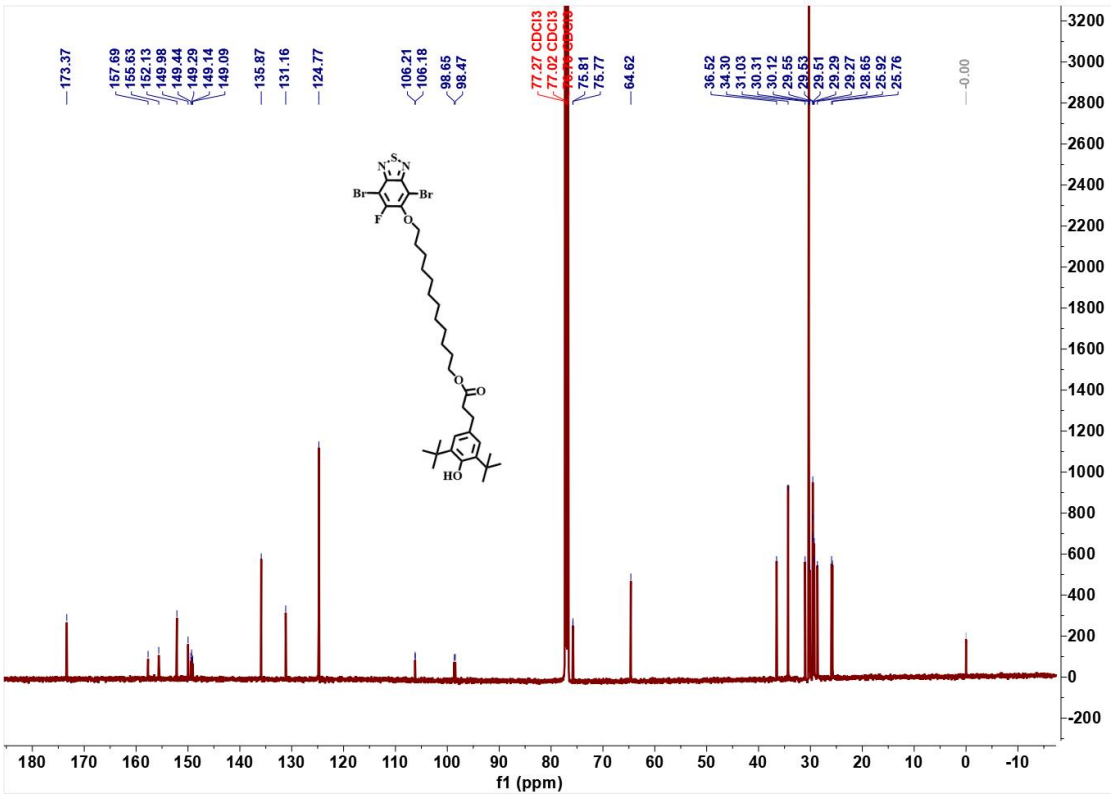

Fig. S7. ^{13}C NMR spectra of compound M1 ($CDCl_3$).

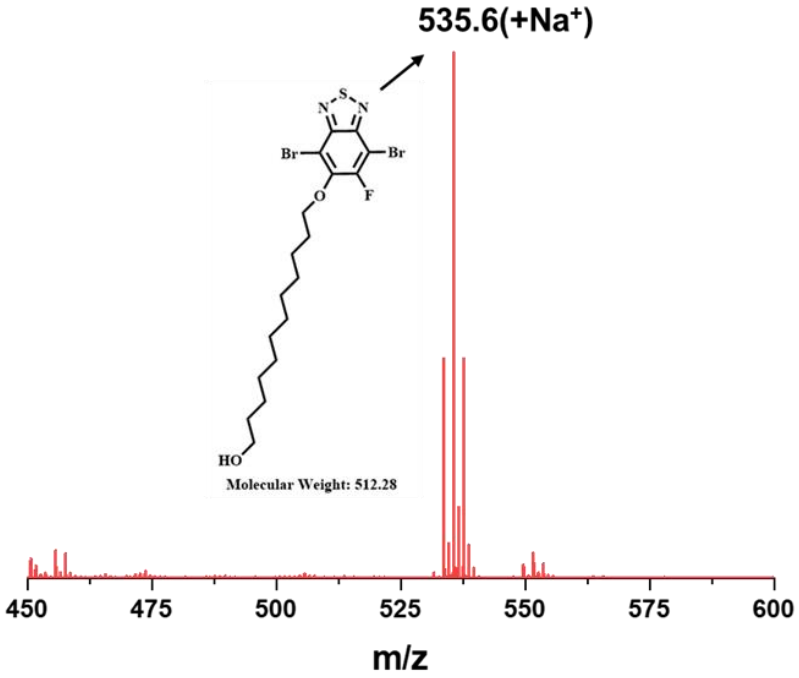

Fig. S8. The mass spectral data of compound 3.

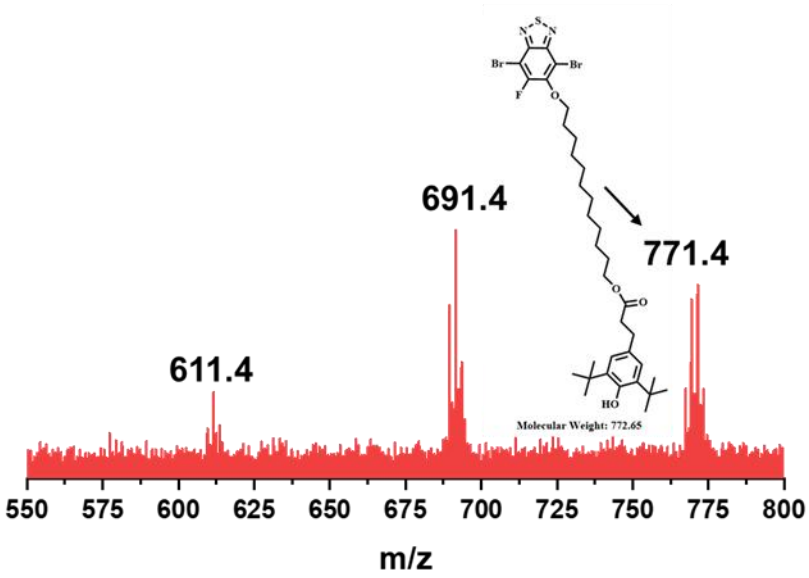

Fig. S9. The mass spectral data of compound M1.

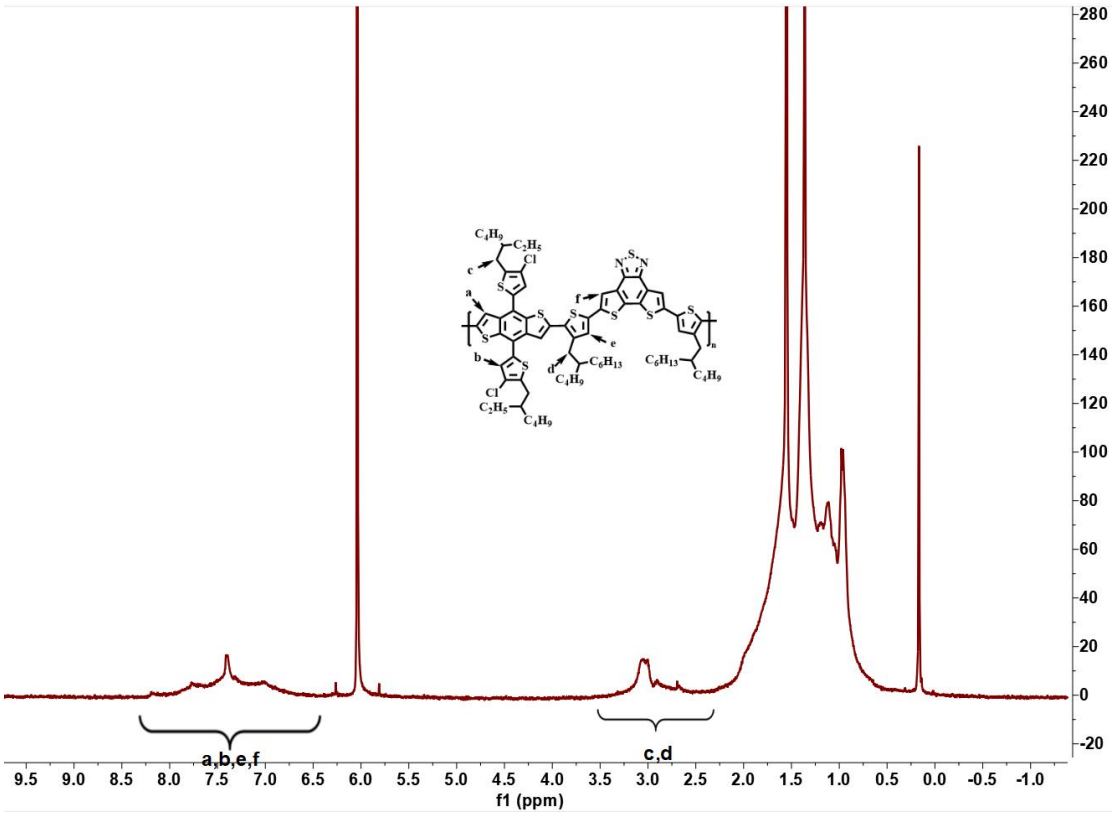

Fig. S10. ^{1}H NMR spectra of D18-Cl (1,1,2,2-$C_2D_2Cl_4$).

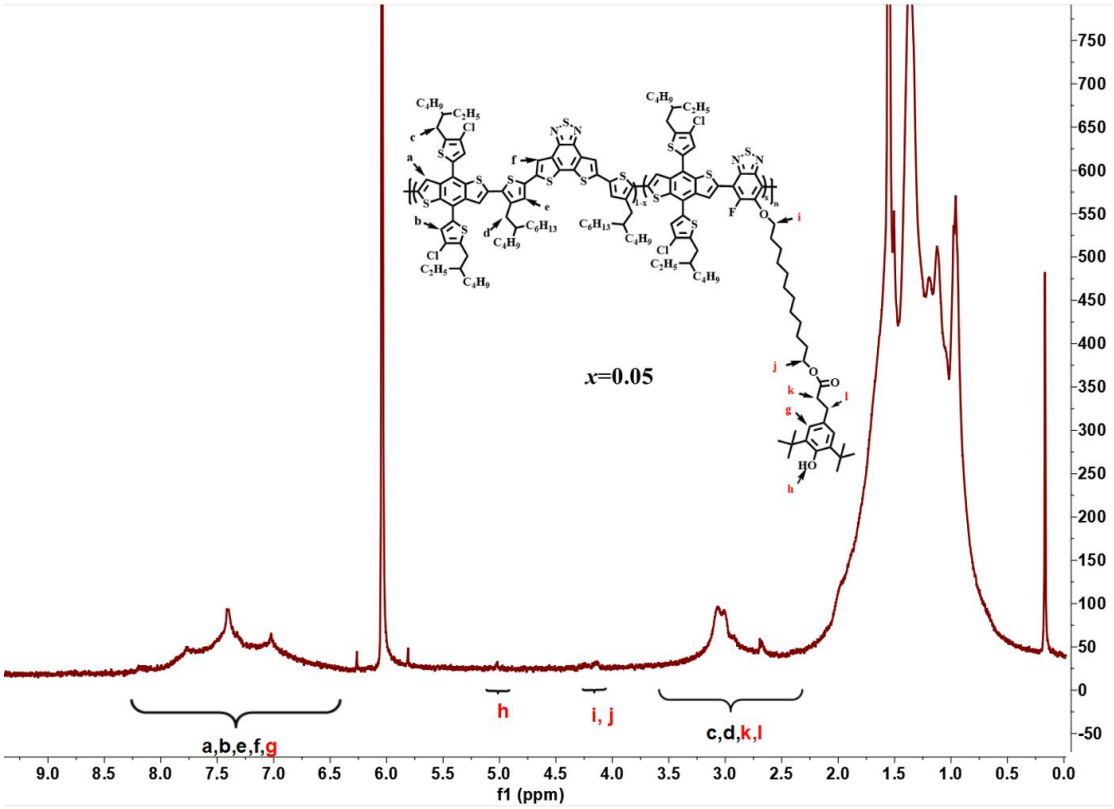

Fig. S11. ^{1}H NMR spectra of D18-Cl-BTBHT0.05 (1,1,2,2-$C_2D_2Cl_4$).

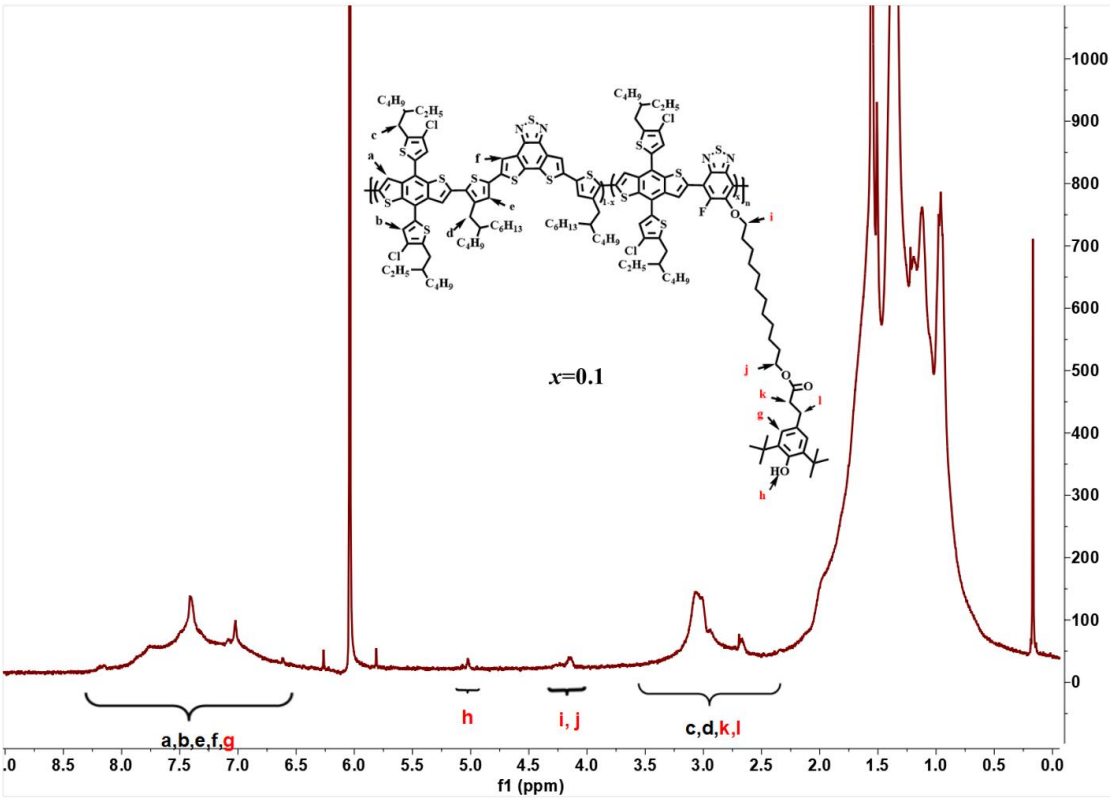

Fig. S12. ^{1}H NMR spectra of D18-Cl-BTBHT0.1 (1,1,2,2-$C_2D_2Cl_4$).

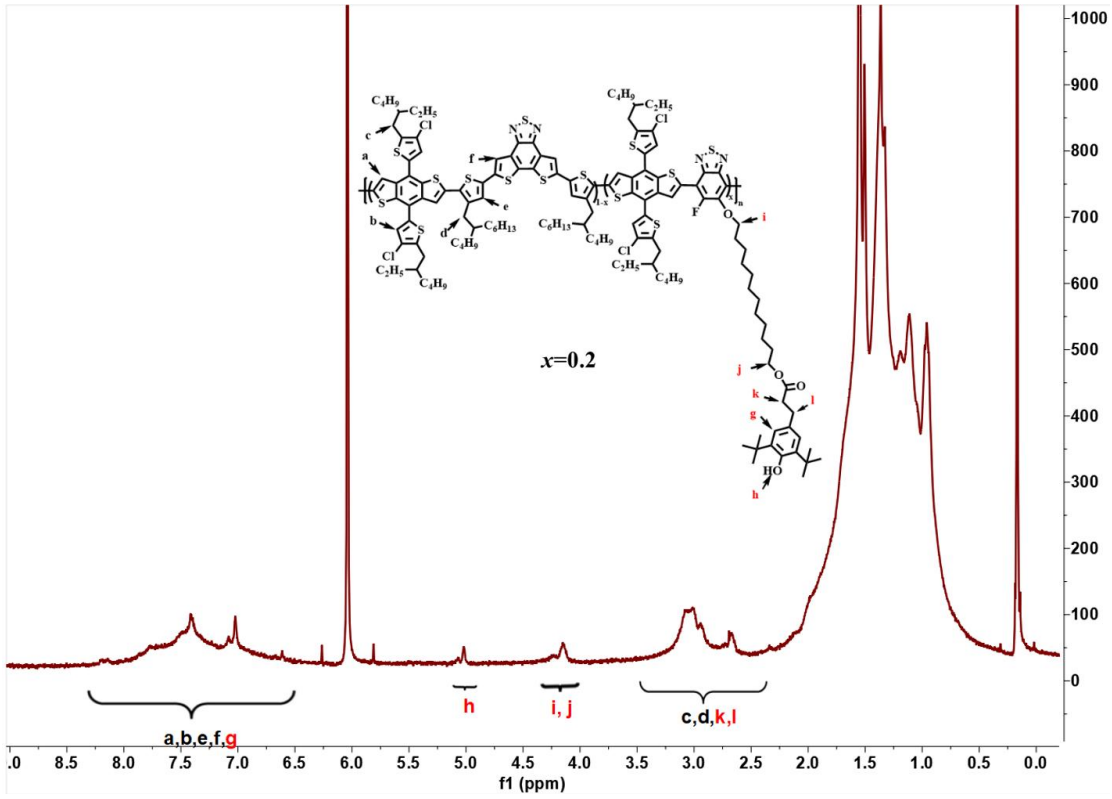

Fig. S13. ^{1}H NMR spectra of D18-Cl-BTBHT0.2 (1,1,2,2-$C_2D_2Cl_4$).

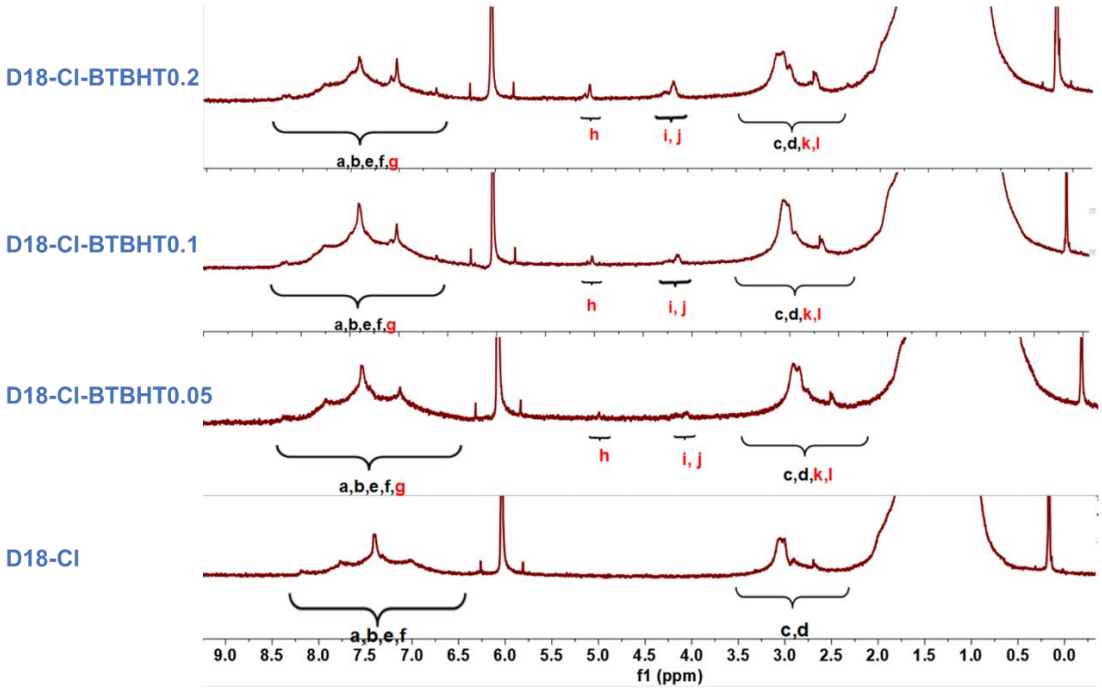

Fig. S14. Comparison of ^{1}H NMR spectra of D18-Cl-BTBHT*x* (1,1,2,2-$C_2D_2Cl_4$).

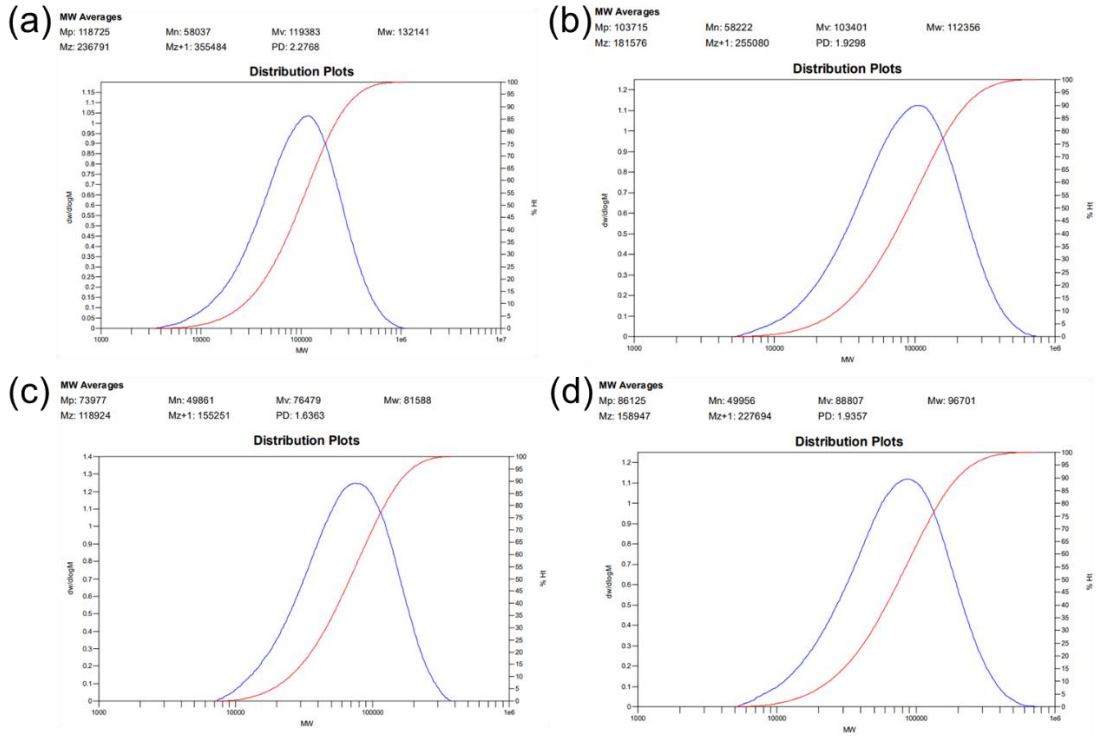

Fig. S15. The GPC trace of (a) D18-Cl, (b) D18-Cl-BTBHT0.05, (c) D18-Cl-BTBHT0.1 and (d) D18-Cl-BTBHT0.2.

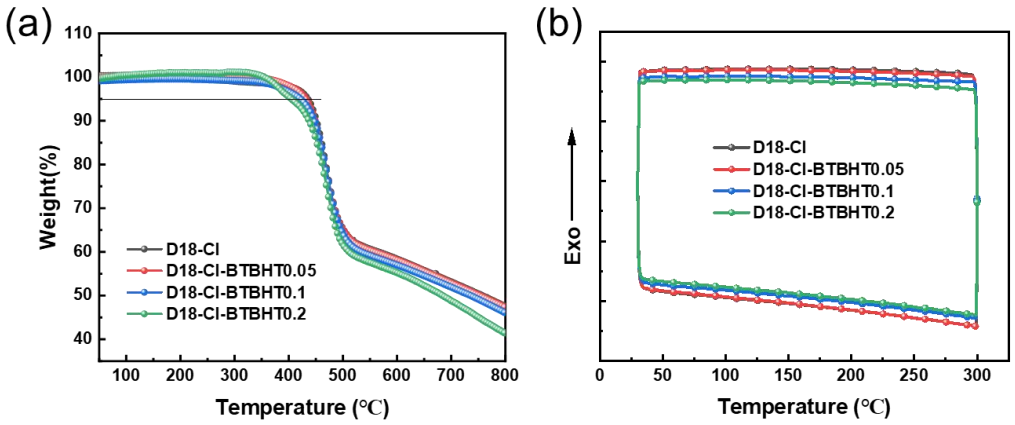

Fig. S16. (a) Thermal gravimetric analysis of donor polymers. (b) DSC traces of donor polymers.

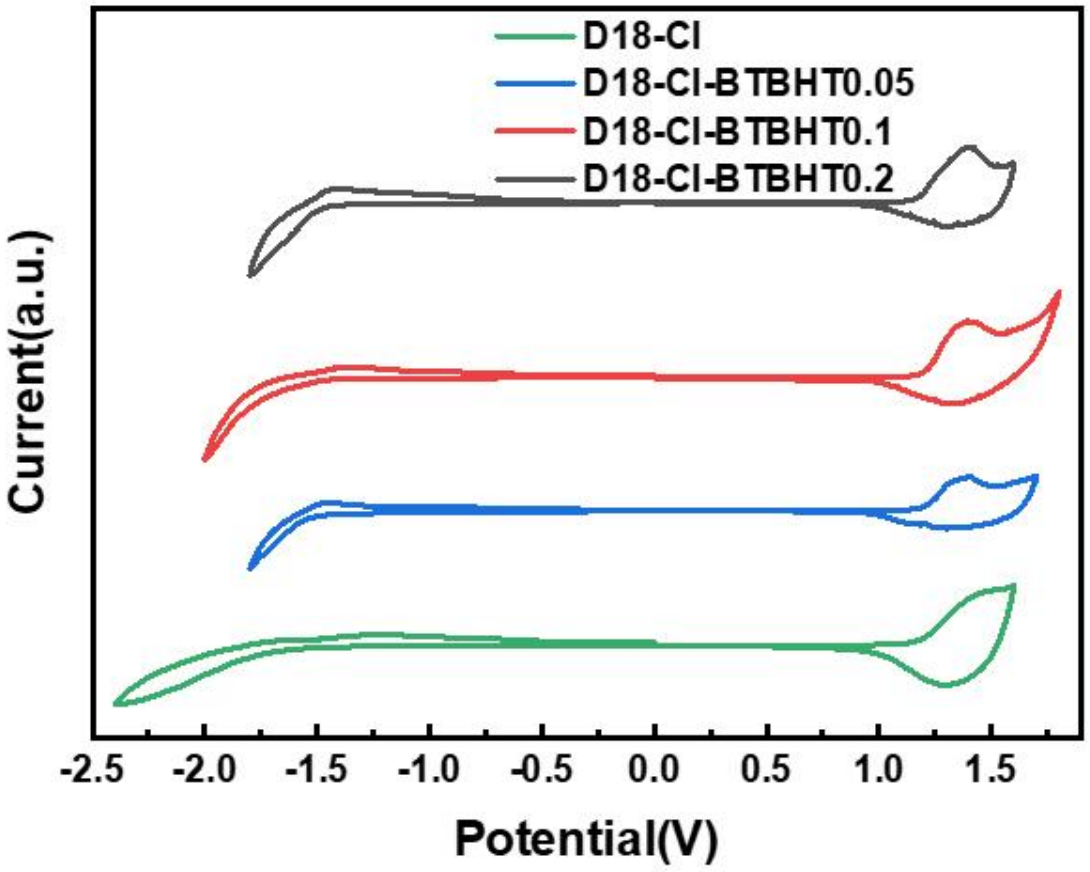

Fig. S17. Cyclic voltammetry curves of donor polymers.

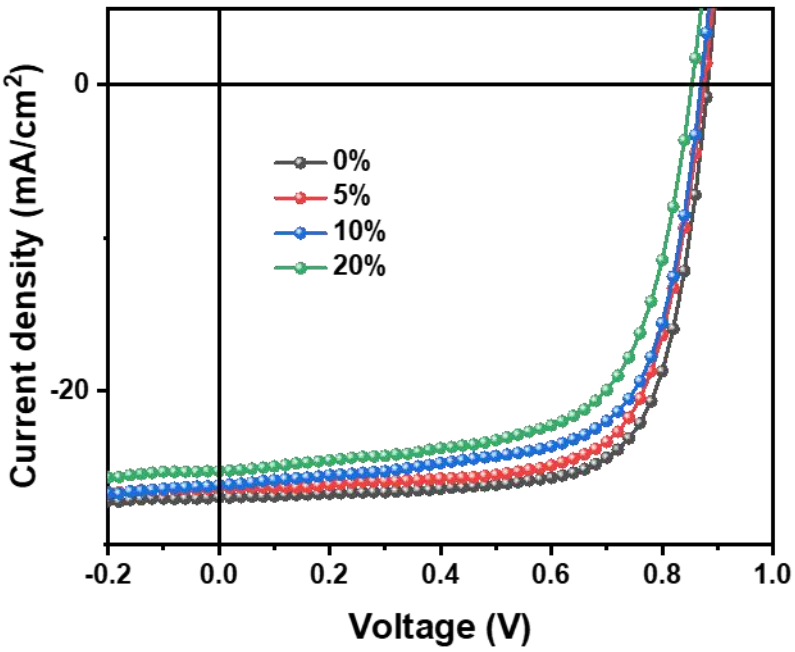

Fig. S18. *J-V* curves of D18-Cl: Y6 cells with BHT doping concentration from 0%-20%.

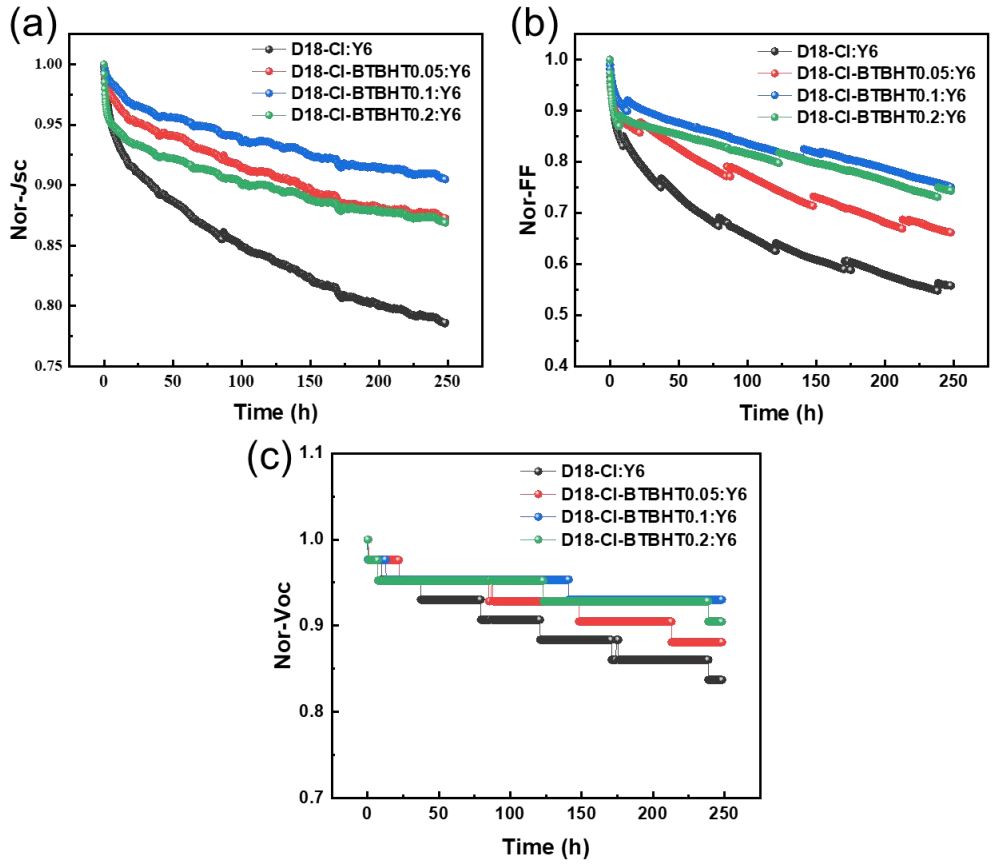

Fig. S19. Evolution of J_{SC}, FF and V_{OC} of D18-Cl-BTBHT*x*: Y6 cells aged at maximum power point with continuous light illumination.

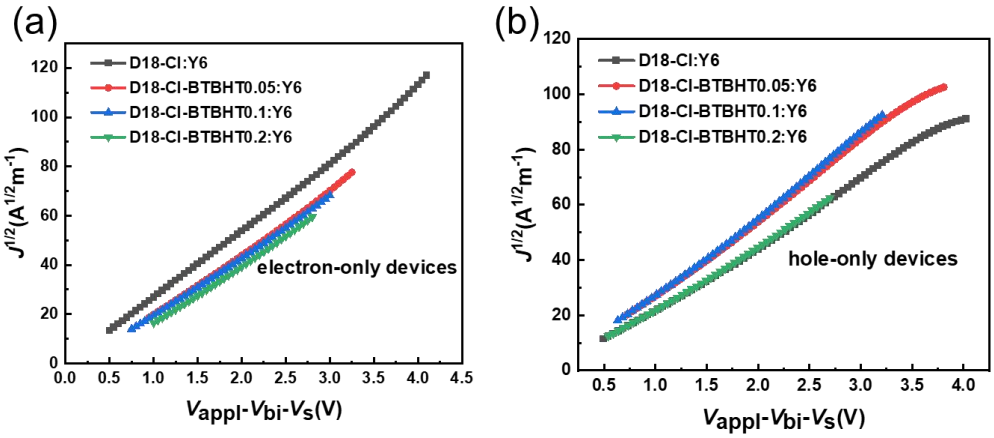

Fig. S20. (a) Electron and (b) Hole Mobility.

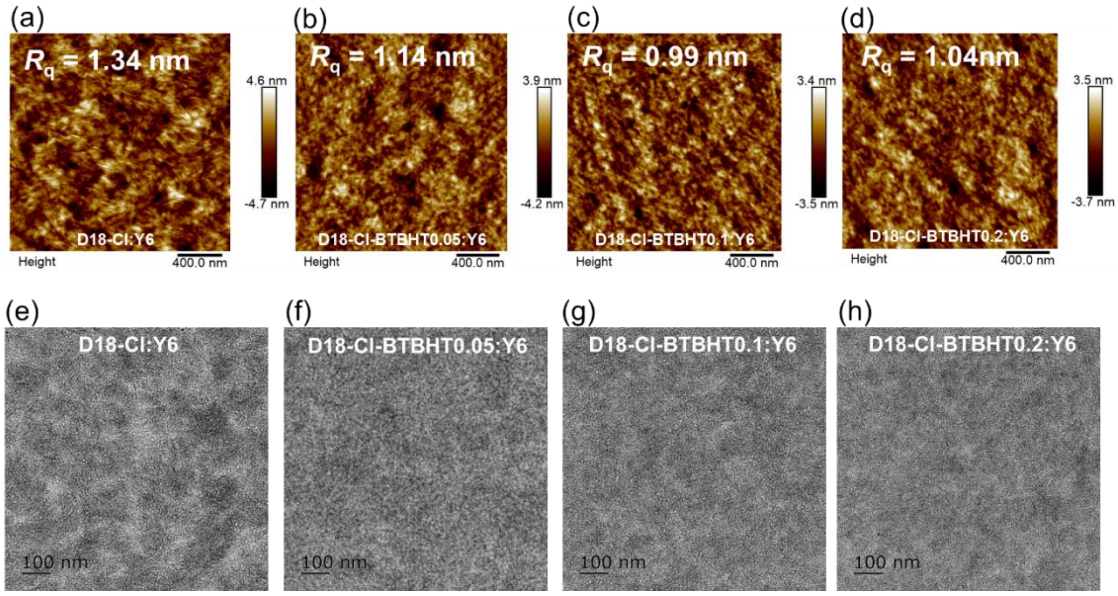

Fig. S21. (a-d) The AFM images of films; (e-h) The TEM images of films.

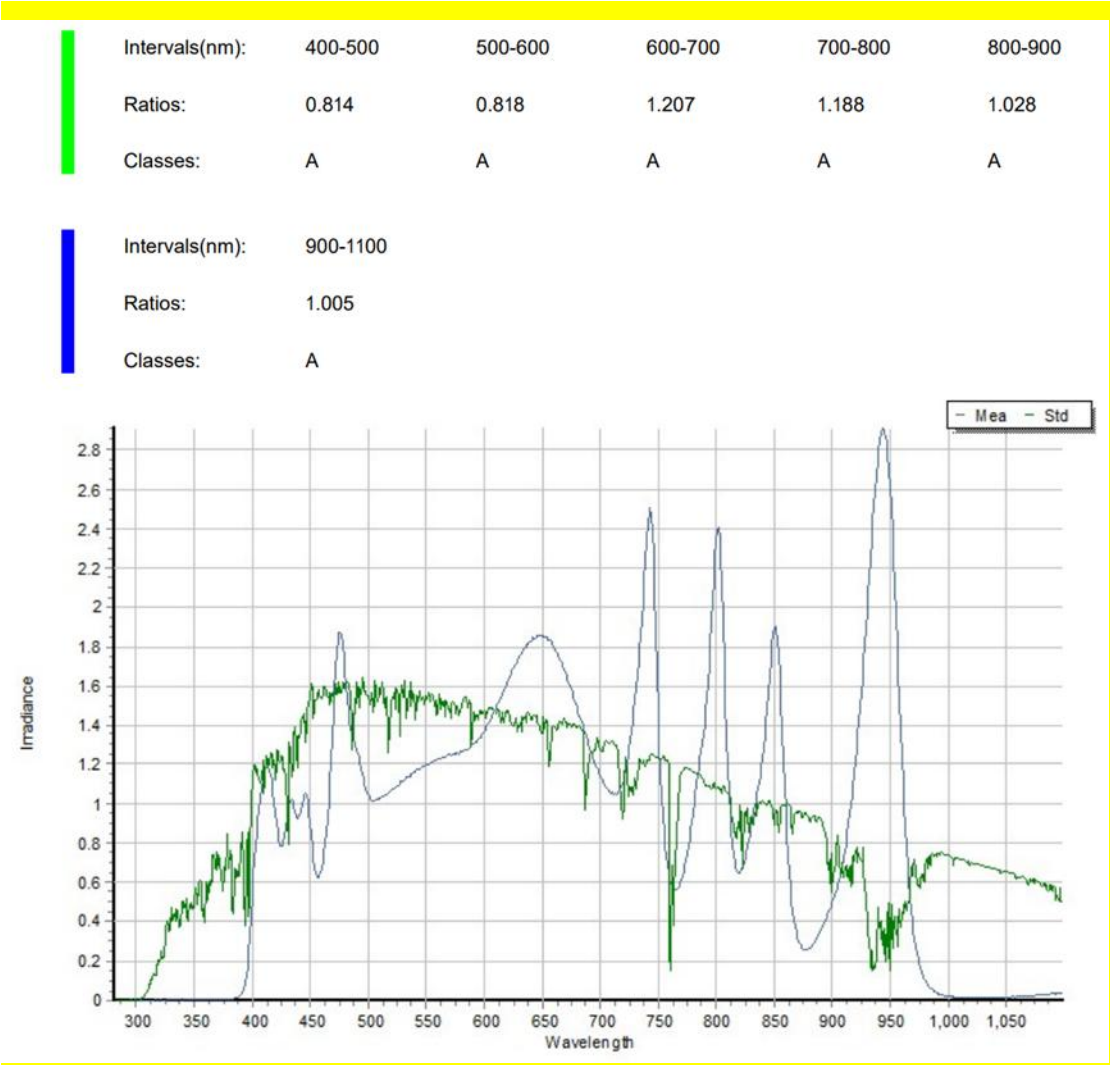

Fig. S22. The spectral of the LED light for stability measurement.

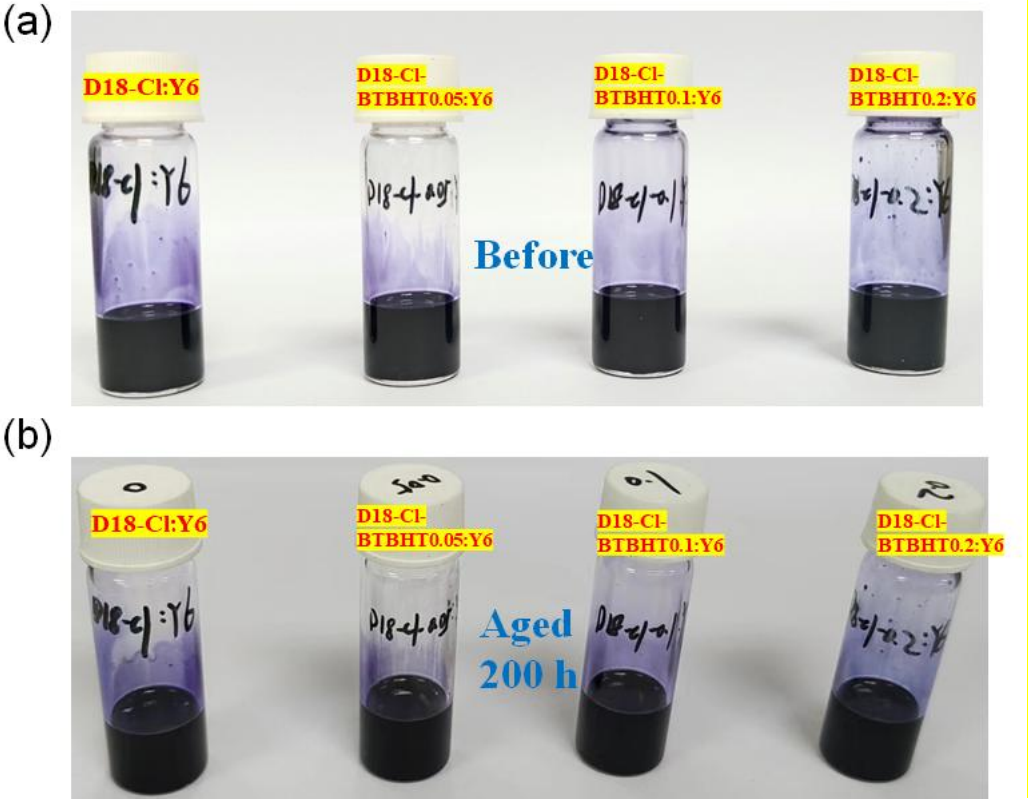

Fig. S23. The photo of mixed solutions before and after aging for 200 h.

Table S1. Photovoltaic parameters of D18-Cl: Y6 solar cells added with BHT weight concentration from 0%-20%.[a]

Active layer	BHT doping ratio	V_{OC} (V)	J_{SC} (mA cm^{-2})	FF (%)	PCE (%)
D18-Cl: Y6	0%	0.89 (0.88±0.00)	26.92 (26.71±0.18)	72.15 (71.57±0.73)	17.13 (16.13±0.31)
D18-Cl: Y6	5%	0.88 0.87±0.00)	26.35 (26.26±0.07)	71.23 (70.46±1.10)	16.32 (17.17±0.41)
D18-Cl: Y6	10%	0.87 (0.87±0.00)	26.13 (25.74±0.36)	70.00 (68.96±1.26)	15.45 (15.41±0.05)
D18-Cl: Y6	20%	0.86 (0.86±0.00)	25.35 (25.12±0.25)	67.69 (66.09±1.46)	14.61 (14.26±0.25)

[a] The average data and the corresponding standard deviation were calculated based on 12 individual devices.

References

[1]Wang Z, Gao K, Kan Y, et al., The coupling and competition of crystallization and phase separation, correlating thermodynamics and kinetics in OPV morphology and performances, Nature Communications, 2021, 12(1): 332